American Journal of Nanosciences
2022; 8(2): 19-30
http://www.sciencepublishinggroup.com/j/ajn
doi: 10.11648/j.ajn.20220802.12
ISSN: 2575-484X (Print); ISSN: 2575-4858 (Online)

A Numerical Approach of the Behavior of a Compound Parabolic Trough Concentrator (CPC) with Double Glazing Using a Nanofluid as Working Fluid

Souleymane Ouedraogo[1, *], Sampawinde Augustin Zongo[1], Jean-Fidele Nzihou[1, 2], Tizane Daho[1], Antoine Bere[1], Bila Gerard Segda[1], Jean Koulidiati[1]

[1]Laboratory of Environmental Physics and Chemistry, Joseph KI-ZERBO University, Ouagadougou, Burkina Faso

[2]Laboratory of Energetic Research and Space Meteorology, Norbert ZONGO University of Koudougou, Koudougou, Burkina Faso

Email address:

souley1010@yahoo.fr (Souleymane O.), zongosaugustin@yahoo.fr (Sampawinde A. Z.), jeanfidele@hotmail.com (Jean-Fidele N.), tizane_daho@yahoo.fr (Tizane D.), berebiya@yahoo.fr (Antoine B.), gsegda@gmail.com (Bila G. S.), jean.koulidiati@gmail.com (Jean K.)

[*]Corresponding author

To cite this article:

Souleymane Ouedraogo, Sampawinde Augustin Zongo, Jean-Fidele Nzihou, Tizane Daho, Antoine Bere, Bila Gerard Segda, Jean Koulidiati. A Numerical Approach of the Behavior of a Compound Parabolic Trough Concentrator (CPC) with Double Glazing Using a Nanofluid as Working Fluid. *American Journal of Nanosciences*. Vol. 8, No. 2, 2022, pp. 19-30. doi: 10.11648/j.ajn.20220802.12

Received: May 26, 2022; **Accepted**: June 25, 2022; **Published**: June 30, 2022

Abstract: The aim of this work is the modeling by a numerical approach of the behavior of a compound parabolic trough concentrator (CPC) with double glazing using a nanofluid as working fluid. The base fluid is jatropha oil for it does not have an ecotoxic impact. The thermal oil, jatropha oil, selected takes into account the constraints related to sustainable development by reconciling ecological, social and economic aspects. The nanofluid used is aluminum oxide having a cylindrical shape with a dimension of 20 nm added to jatropha oil (Al_2O_3+jatropha oil). The volume fraction of the nanofluid is 10%. The numerical model developed is based on the detailed analysis of the different forms of heat transfer that occur in the CPC. The equilibrium equations for each element of the system have been set up. The different heat exchanges that took place in each compartment of the CPC were described. The heat transfer equations were solved by the Gauss-Seidel's method. An advanced difference scheme is used for the storage terms and a decentered scheme for the transport terms. The numerical simulation has been implemented by matlab code. The effects of varying the mass flow rate and the width of the CPC canopy on the different parameters such as the fluid outlet temperature and the thermal efficiency of the collector are analyzed. The theoretical results showed that the lower the mass flow rate, the higher the fluid outlet temperature and thermal efficiency. They also establish that as the width increases the fluid temperature and thermal efficiency increases. The opening angle and the reflectance coefficient have an influence on the CPC operation. The higher these two parameters are, the higher the output temperature.

Keywords: CPC, Daily Efficiency, Nanofluid, Numerical Simulation, Mass Flow, Outlet Temperature

1. Introduction

The compound parabolic trough concentrator (CPC) is one of the types of solar collectors that can capture solar radiation on the media concentrated in one point, and then converted into thermal energy that can be applied in the power generation system. Much research has been conducted on CPC using various working fluids. Some studies developed a CPC to heat the working fluid as methanol. The CPC can absorb solar energy with a maximum efficiency of 80% [1]. Thus, the heat transfer efficiency can also be improved by increasing the thermal conductivity of the heat transfer fluid. The thermal conductivity of fluids commonly used in heat transfer, such as water, ethylene glycol, and oils is relatively low, compared to the thermal conductivity of solids. In this regard, various techniques have been proposed to modify the thermophysical properties of fluids. Among these techniques, one of them mention that of increasing the thermal conductivity of base fluids, such as ethylene glycol, water and oils, by suspending solid nanoparticles in these fluids. These techniques have given rise to a new class of heat

transfer fluids, called nanofluids.

In the last few years, nanofluids have attracted great interest due to their use for cooling. The use of nanofluids increases the natural convection heat transfer in a remarkable way with a huge possibility of replacing the traditional fluids and oils used until now for cooling [2]. Nanofluids are becoming promising thermofluids for heat transfer applications. Nanofluids are two-phase fluids with a liquid-solid mixture. The presence of solid nanoparticles in the base fluid significantly increases the effective thermal conductivity of the fluid and therefore improves the heat transfer characteristics [3]. The addition of a single nanoparticle to the base fluid to improve the flow and heat transfer characteristics of the base fluid is a proven technology.

In recent years, attention has focused on research studies involving the impregnation of two or more nanoparticles into base fluids, referred to as hybrid or composite nanofluids. Çolak and al. (2020) developed an artificial neural network model to estimate the specific heat of the Cu-Al_2O_3/water hybrid nanofluid as a function of temperature and volume concentration [4]. Convection of a hybrid nanofluid in a permeable medium was presented by Nguyen and al. (2019) with CVFEM (control volume finite element method) with magnetic effect. Hybrid nanoparticles (Fe_3O_4 + MWCNT) with a water base fluid were considered. The impacts of Darcy number, magnetism, radiation and Rayleigh number on the migration of nanomaterials have been described [5]. The problem of mixed convection in a porous trapezoidal cavity filled with a hybrid nanofluid (Cu-Al_2O_3/water) has been done by Cimpean and al. (2020) and numerical results have been obtained and discussed [6]. Adun and al (2020) addressed some of the challenges in predicting the characteristics of hybrid nanofluids by using datasets from several experimental investigations on various hybrid nanofluids to form an intelligent neural network [7].

The purpose of this work is to estimate the possibilities of heat transfer enhancement by using nanofluids. We have grasped the fundamental mechanisms involved in these heat transfer modes from a theoretical approach by simulation of the CPC thermal parameters. The nanofluid used is aluminum oxide having a cylindrical shape with a dimension of 20 nm added to jatropha oil (Al_2O_3+jatropha oil). The volume fraction of the nanofluid is 10%. The study of the behavior of the CPC with double glazing using a nanofluid as working fluid is of great importance because it allows to simulate the level of temperature reached by the CPC i.e. its capacity and its rate of vaporization with this type of working fluid. It is shown that nanofluids have the possibility to increase the transfer capacity of heat exchangers without having to increase their useful volume. The theoretical results showed that the lower the mass flow rate, the higher the fluid outlet temperature and thermal efficiency. They also establish that as the width increases the fluid temperature and thermal efficiency increases. The opening angle and the reflectance coefficient have an influence on the CPC operation. The higher these two parameters are, the higher the output temperature.

2. Thermophysical Properties of the Nanofluid

2.1. The Volume Fraction

This is the most important property for a nanofluid, it is defined as the ratio of the volume of dispersed nanoparticles (Vs) to the total volume (VT). The value of the volume fraction varies from 0 (pure base fluid) and 1 (fully nanoparticles). The relationship is given as follows:

$$\chi = \frac{V_S}{V_T} = \frac{V_S}{V_S + V_f} \tag{1}$$

2.2. The Density

The density is calculated by a classical relationship of Xuan and Roetzel as follows [8]:

$$\rho_{nf} = \chi\rho_S + (1-\chi)\rho_f \tag{2}$$

2.3. The Specific Heat

The specific heat is defined by two formulas, one is that of Roetzel and Xuan given as a function of density, it is defined as follows [8]:

$$(\rho C_p)_{nf} = \chi(\rho C_p)_s + (1-\chi)(\rho C_p)_f \tag{3}$$

On the other hand, Pak and Cho present the specific heat of nanofluids under the following equation [9]:

$$C_{Pnf} = (1-\chi)C_{Pf} + \chi C_{Pp} \tag{4}$$

2.4. The Dynamic Viscosity

Einstein was the first to study the dynamic viscosity of a mixture containing dilute suspensions of fine spherical and rigid particles in low volume concentration (less than 0.02). The relationship is presented as follows [10]:

$$\frac{\mu_{nf}}{\mu_f} = 1 + 2.5\chi \tag{5}$$

Brinkman extended Einstein's formula to cover a wide range of volume concentrations. His relation leads to the Einstein relation for low volume fractions [11]:

$$\frac{\mu_{nf}}{\mu_f} = \frac{1}{(1-\chi)^{2.5}} \tag{6}$$

Batchelor theoretically studied the dynamic viscosity of a nanofluid taking into account the effect of hydrodynamic interaction between two spherical nanoparticles, he showed that the dynamic viscosity of a nanofluid is not a linear function of the volume fraction like the relations of "Einstein and Brinkman" [12]]:

$$\mu_{nf} = \mu_f(1 + 2.5\chi + 6.2\chi^2) \tag{7}$$

Maiga and al. presented experimentally the dynamic viscosity of alumina nanoparticles dispersed in water and ethylene glycol. The correlation of the dynamic viscosity of the nanofluid

(Al_2O_3/water) was identical to equation (8) for the other nanofluid the relationship is identified as follows [13]:

$$\mu_{nf} = \mu_f(1 + 7.3\chi + 123\chi^2) \quad (8)$$

The Pak and Cho Model gives the dynamic viscosity by the following relationship:

$$\mu_{nf} = \mu_f(1 + 39.11\chi + 533.9\chi^2) \quad (9)$$

2.5. The Thermal Conductivity

Maxwell theoretically studied the thermal conductivity of a nanofluid containing only spherical nanoparticles. He assumed that the particles have the same diameter and they are separated by a sufficient distance leading to the absence of mutual interaction between them, the thermal conductivity in his model depends only on the volume fraction of the suspended nanoparticles, the thermal conductivity of the base fluid and that of the nanoparticles [14]:

$$\frac{\lambda_{nf}}{\lambda_f} = \frac{\lambda_P + 2\lambda_f - 2\chi(\lambda_f - \lambda_P)}{\lambda_P + 2\lambda_f + \chi(\lambda_f - \lambda_P)} \quad (10)$$

Yu and Choi proposed a new formula to calculate the conductivity of a nanofluid. They proposed to model nanofluids as a base liquid and solid particles separated by a nanoscale layer, this layer acts as a thermal bridge between the fluid and the nanoparticles. In addition they assumed that the thermal conductivity of the nanoscale layer is higher than that of the liquid.

$$\frac{\lambda_{nf}}{\lambda_f} = \frac{\lambda_P + 2\lambda_f - 2\chi(\lambda_f - \lambda_P)(1+\beta)^3}{\lambda_P + 2\lambda_f + \chi(\lambda_f - \lambda_P)(1+\beta)^3} \quad (11)$$

Lu and Lin proposed a new formula for any shape of the nanoparticles by introducing variables depending on the thermal conductivity of the dispersed nanoparticles, the relationship being given as follows [15]:

$$\frac{\lambda_{nf}}{\lambda_f} = 1 + a\,\chi + b\chi^2 \quad (12)$$

$\lambda_p = 10$	a=2.25	b=2.27
$\lambda_p > 10$	a=3.00	b=4.51

Keblinski and al. investigated the conductivity of several nanofluids and the mechanisms contributing to the increase of this property. They presented the following empirical relationships [16]:

2.5.1. For the Nanofluid: EG + Al_2O_3

$$\lambda_{nf} = \lambda_f(1 + 2.8273\chi + 28.905\chi^2) \quad (13)$$

2.5.2. For the Nanofluid: Water + Al_2O_3

$$\lambda_{nf} = \lambda_f(1 + 6.3\chi - 13\chi^2) \quad (14)$$

2.5.3. For the Nanofluid: Cu + Water

$$\lambda_{nf} = \lambda_f(1 + 9.6\chi + 11.6\chi^2) \quad (15)$$

Timofeeva et al. experimentally and theoretically studied the thermal conductivity of Al_2O_3 in water and Al_2O_3 in ethylene glycol, they reported a correlation that depends only on the thermal conductivity of the base fluid and the volume concentration of the suspended alumina [17]:

$$\lambda_{nf} = \lambda_f(1 + 3\chi) \quad (16)$$

3. CPC Modeling

3.1. Schemes

Figures 1 and 2 below show the CPC diagrams.

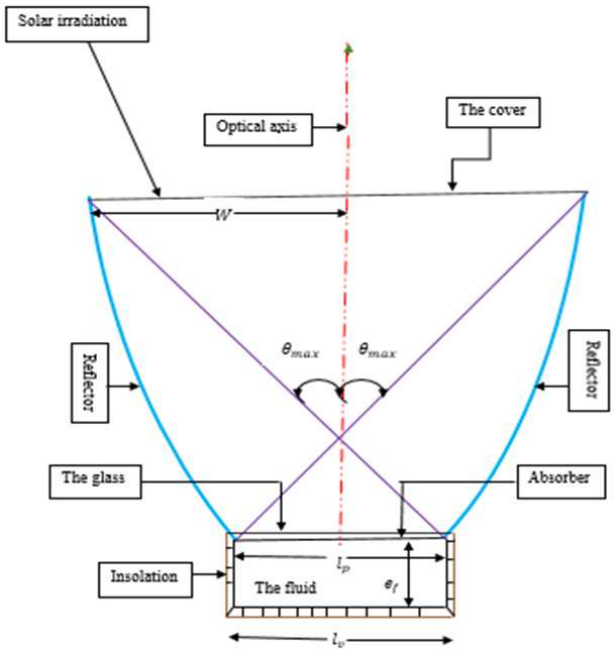

Figure 1. *Scheme of the system.*

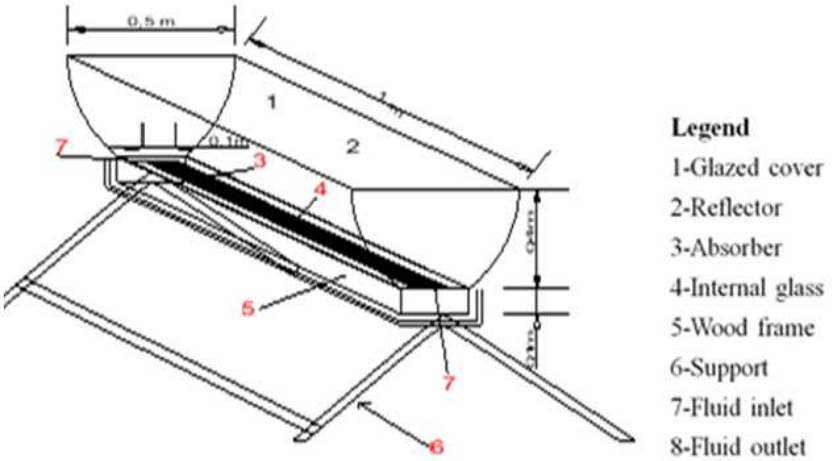

Figure 2. *Schematic diagram of CPC.*

The soltrace software code uses a methodology of tracing a specified number of solar rays from the sun through the system, and each of them passes through the defined system encountering various optical interactions. The figure 3 below shows the modeling of the solar rays passing through the CPC.

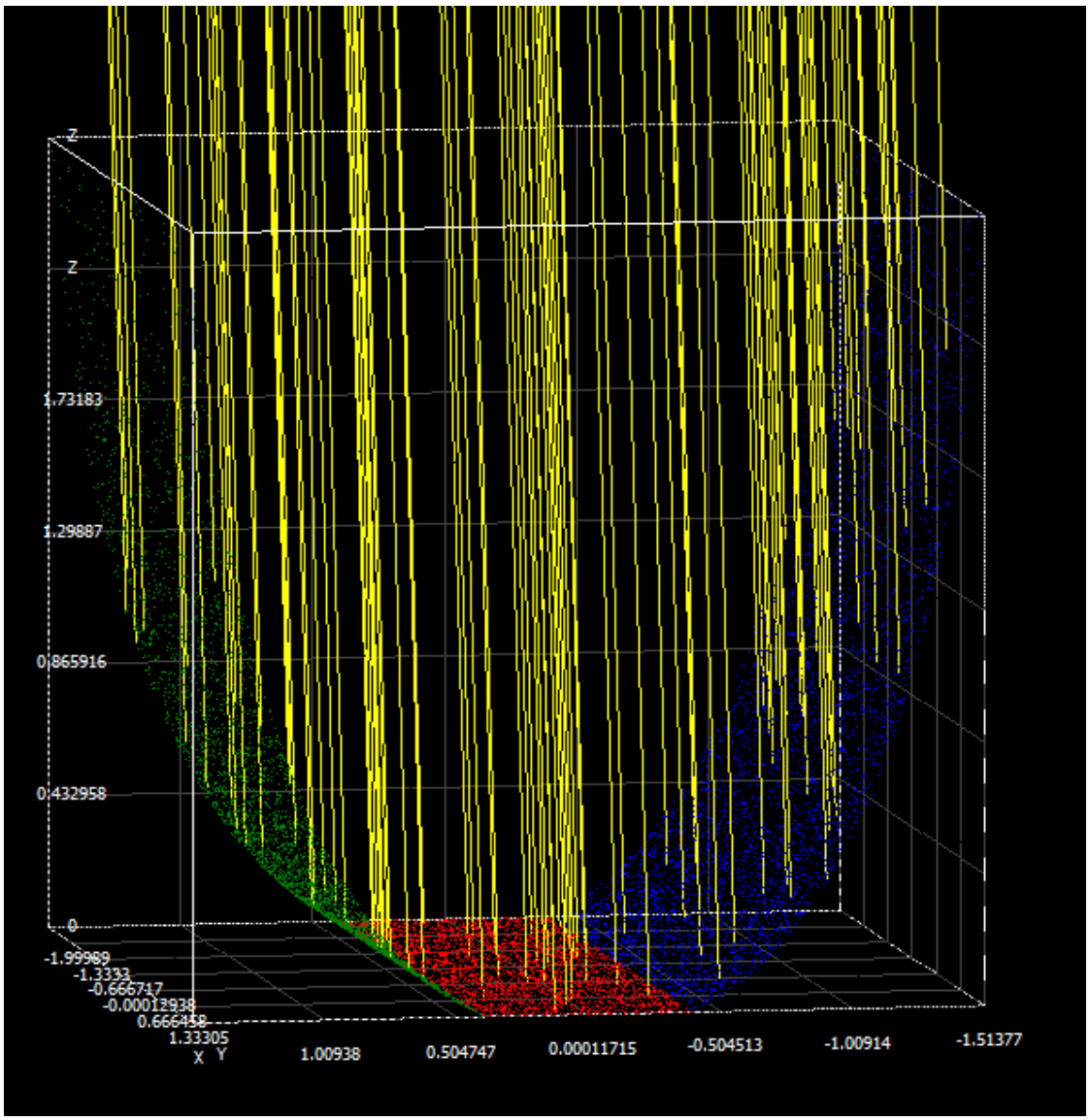

Figure 3. *Modeling of the solar rays passing through the CPC.*

3.2. Simplifying Assumptions

The balance equations that will be established in the following are based on the following simplifying assumptions:

1) Lateral and rear heat transfers are assumed to be negligible;
2) The vertical and axial heat conductions are assumed to be negligible, each component is represented by a single temperature;
3) The external and internal convective exchange coefficients are assumed to be constant over the entire length of the collector;
4) The pressure losses are neglected;
5) The absorber is represented by a steel sheet painted in black to absorb a maximum of energy.

3.3. The Thermal Balance Equations of the Collector

The different equations obtained are [18]:

3.3.1. At the Cover Level

The glazed canopy receives direct and diffuse radiation on its upper surface and exchanges by convection and radiation with the surrounding environment.

$$M_c C_c \frac{\partial T_c(x,t)}{\partial t} = Q_c(x,t) + \left(h_{r,c-v} + h_{c,c-v}\right)(T_v - T_c) - h_{r,c-ciel}(T_c - T_{ciel}) - h_v(T_c - T_a) \quad (17)$$

3.3.2. At the Glass Level

Similarly, the energy balance for the glass is given by:

$$M_v C_v \frac{\partial T_v(x,t)}{\partial t} = Q_v(x,t) + h_{r,p-v}\left(T_p - T_v\right) - h_{c,c-v}\,(T_v - T_c) - h_{r,c-v}\,(T_v - T_c) \quad (18)$$

3.3.3. At the Absorber Level

The energy balance for the absorber is obtained by the following expression:

$$M_p C_p \frac{\partial T_p(x,t)}{\partial t} = Q_p(x,t) - h_{r,p-v}.\left(T_p - T_v\right) - h_{c,p-f}\left(T_p - T_f\right) \quad (19)$$

3.3.4. At the Fluid Level

The energy balance for the heat transfer fluid flowing through the absorber tube is given by the following relationship:

$$\rho_f C_f e_f \frac{\partial T_f(x,t)}{\partial t} = -\frac{\dot{m}_f C_f}{l_p}\frac{\partial T_f(x,t)}{\partial x} + h_{c,p-f}\left(T_p - T_f\right) \quad (20)$$

3.4. Expressions of Heat Transfer Coefficients

As a reminder, there are three well known modes of heat exchange; convective, radiative and conductive. To draw up a complete balance of the transfers that took place in the concentrator we must consider the mode of flow of the fluid and the architecture of the device. In our study, we have neglected the heat transfer by conduction.

3.4.1. Coefficient of Exchange by Radiation the Sky Vault and the Glass

The radiation exchange coefficient between the sky and the glass is given by the following expression:

$$h_{r,c-ciel} = \sigma\varepsilon_c(T_c^2 + T_{ciel}^2)(T_c + T_{ciel})\frac{A_c}{A_p} \quad (21)$$

3.4.2. Convective Exchange Coefficient Due to Wind

The exchange coefficient between the external environment and the glass is given by the formula of Mac Adams formula [19]:

$$h_v = (5.7 + 3.8V)\frac{A_c}{A_p} \quad (22)$$

3.4.3. Transfer Coefficient Between the Cover and the Glass

There are two thermal exchanges between the glass and the cover. One by radiation and the other by convection.

3.4.4. Radiation Exchange Coefficient Between the Canopy and the Glass

The radiation exchange coefficient between the canopy and the glass is given by the following expression [20]:

$$h_{r,c-v} = \frac{\sigma\varepsilon_c(T_c^2+T_v^2)(T_c+T_v)\frac{A_c}{A_p}}{\frac{1}{\varepsilon_v}+\frac{A_v}{A_c}(\frac{1}{\varepsilon_c}-1)} \quad (23)$$

3.4.5. Coefficient of Exchange by Convection Between the Cover and the Glass

The convective transfer coefficient between the canopy and the glass is given by the following relationship [20]:

$$h_{c,c-v} = (3.25 + 0.085\frac{T_v - T_c}{2D_v})\frac{A_c}{A_p} \quad (24)$$

With

$$D_h = \frac{2l_v(e_f + e_{p-v})}{l_v + e_f + e_{p-v}} \quad (25)$$

3.4.6. Transfer Coefficient Between the Glass and the Absorber

There is a heat exchange between the glass and the absorber. It is the solar radiation between the glass and the absorber. It is given by the following expression:

$$h_{r,p-v} = \frac{\sigma(T_p^2+T_v^2)(T_p+T_v)}{\frac{1}{\varepsilon_p}+\frac{A_p}{A_v}(\frac{1}{\varepsilon_v}-1)} \quad (26)$$

3.4.7. Convection Exchange Coefficient Between the Absorber Plate and the Fluid

The heat transfer fluid exchanges heat with the absorber by

convection. Correlations have been established for the calculation of the Nusselt number according to the nature of the fluid and the flow regime. In our case, the flow regime is laminar. For the calculation of the Nusselt number, we used the following relation:

$$Nu_f = 4.9 + \frac{0.0606(R_e P_r D_h/L)^{1.2}}{1+0.0909(R_e P_r D_h/L)^{0.7} {P_r}^{0.17}} \quad (27)$$

with:

$$R_e = \frac{\dot{m}_f D_h}{l_p e_f \mu_f} \quad (28)$$

$$P_r = \frac{\mu_f}{\lambda_f} C_f \quad (29)$$

$$D_h = \frac{2 l_p e_f}{l_p + e_f} \quad (30)$$

The exchange coefficient is given by:

$$h_{c,p-f} = \frac{\lambda_f}{D_h} Nu_f \quad (31)$$

3.5. Heat Quantity Expressions

According to Hsieh's theory the different heat quantity expressions of the CPC elements are given by the following formulas [20]:

3.5.1. The Quantity of Heat Absorbed by the Canopy

It is given by the following expression:

$$Q_c(t) = DNI\left[\overline{\alpha_c} + \overline{\alpha_c \tau_c} {\zeta_m}^{2<n>}\right] \frac{A_c}{A_p} \quad (32)$$

$$A_c = 2WL \quad (33)$$

$$A_p = L_p l_p \quad (34)$$

The number of reflection means is given by the following formula [20]:

$$< n >= 1 + 0.7 * Cg \quad (35)$$

3.5.2. The Amount of Heat Absorbed by the Glass

$$Q_v(t) = DNI\overline{\tau_c}{\rho_m}^{<n>}\overline{\tau_v}\left[\overline{\alpha_v} + \overline{\alpha_v \rho_v \rho_c}{\zeta_m}^{2<n>}\frac{A_v}{A_c} + \overline{\alpha_v}\overline{\zeta_p}\overline{\tau_v}\right]\frac{A_c}{A_p} \quad (36)$$

$$A_v = L_v l_v \quad (37)$$

3.5.3. The Amount of Heat Absorbed by the Absorber Plate

$$Q_p(t) = DNI\overline{\tau_c}{\rho_m}^{<n>}\overline{\tau_v}\left[\overline{\alpha_p} + \overline{\alpha_p \rho_v \rho_p}\frac{A_p}{A_v}\right]\frac{A_c}{A_p} \quad (38)$$

4. Numerical Results and Discussions

The balance equations described above are coupled and the consideration of radiation gives them a non-linear character. An advanced difference scheme is used for the storage terms and a decentered scheme for the transport terms. The Gauss Seidel method is used for the numerical solution. The matlab language has been used for programming the equations.

In the calculation, it was assumed that the solar radiation falls normally in the aperture plane. We assumed that all radiation falls directly into the aperture. For the calculations, the wind speed v = 5m/s was kept constant. The inlet temperature of the fluid takes the value of the ambient temperature, which varies with time. The dimensions and thermophysical properties of the CPC module, for which the numerical simulation was carried out, are presented in the tables attached below. Figure 4 shows the temperatures of the different components of the collector vary according to the solar radiation.

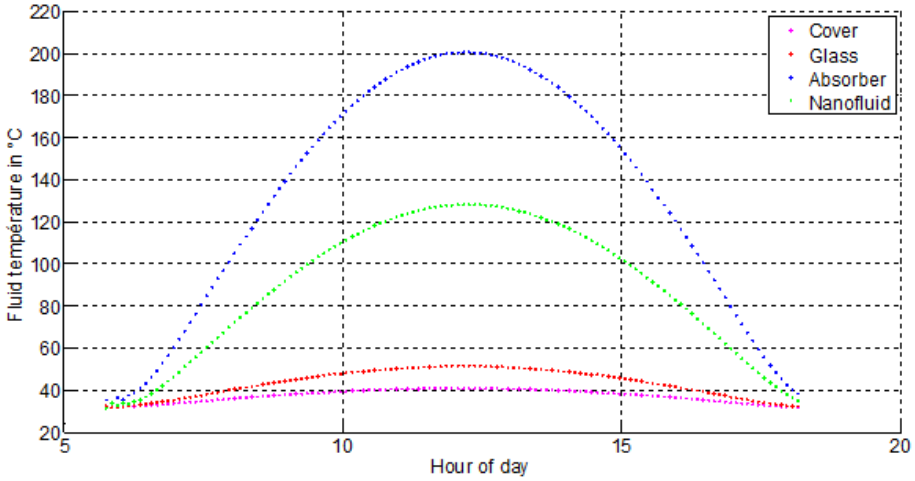

Figure 4. *Temperature of the different components of the collector.*

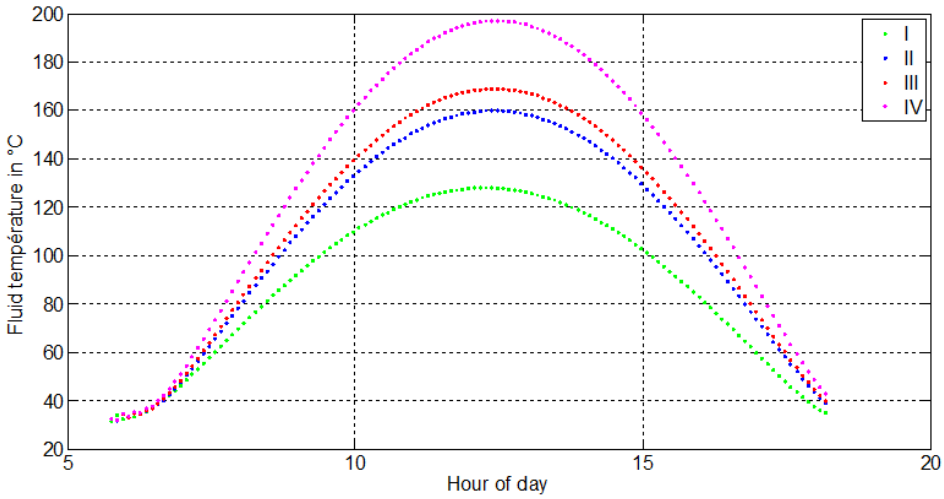

Figure 5. *Impact of mass flow rate on fluid temperature I-$\dot{m}$=9.5x10^{-3} kg/s II-$\dot{m}$=7.2x10^{-3} kg/s III-$\dot{m}$=6.9x10^{-3} kg/s IV-$\dot{m}$=5.8x10^{-3} kg/s.*

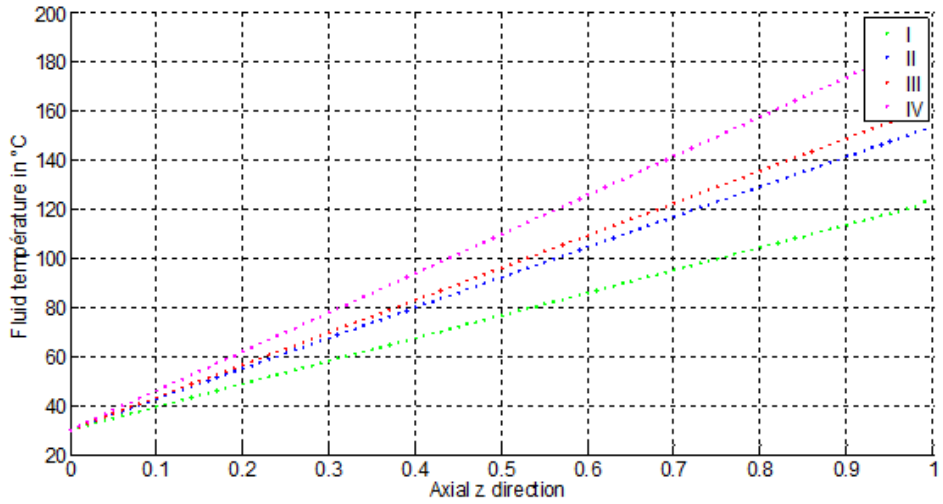

Figure 6. *Impact of the mass flow rate on the temperature of the fluid in the flow direction. I-$\dot{m}$=9.5x10-3 kg/s II-$\dot{m}$=7.2x10-3 kg/s III-$\dot{m}$=6.9x10-3 kg/s IV-$\dot{m}$=5.8x10-3 kg/s.*

Figure 6 shows the impact of mass flow rate on the temperature of the fluid in the flow direction. The temperature of the nanofluid grows linearly with the axial direction. However, the lower the flow rate, the higher the fluid temperature.

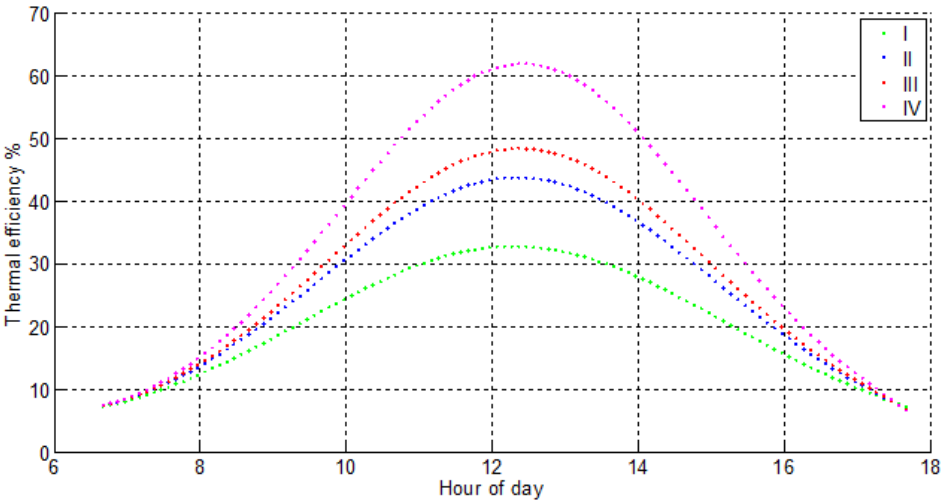

Figure 7. *Impact of the mass flow rate on the thermal efficiency of the fluid I-$\dot{m}$=9.5x10^{-3} kg/s II-$\dot{m}$=7.2x10^{-3} kg/s III-$\dot{m}$=6.9x10^{-3} kg/s IV-$\dot{m}$=5.8x10^{-3} kg/s.*

Figure 7 shows the behavior of the mass flow rate on the thermal efficiency of the fluid as a function of time. It clearly illustrates that if the flow rate is very high, the thermal efficiency of the fluid is very low.

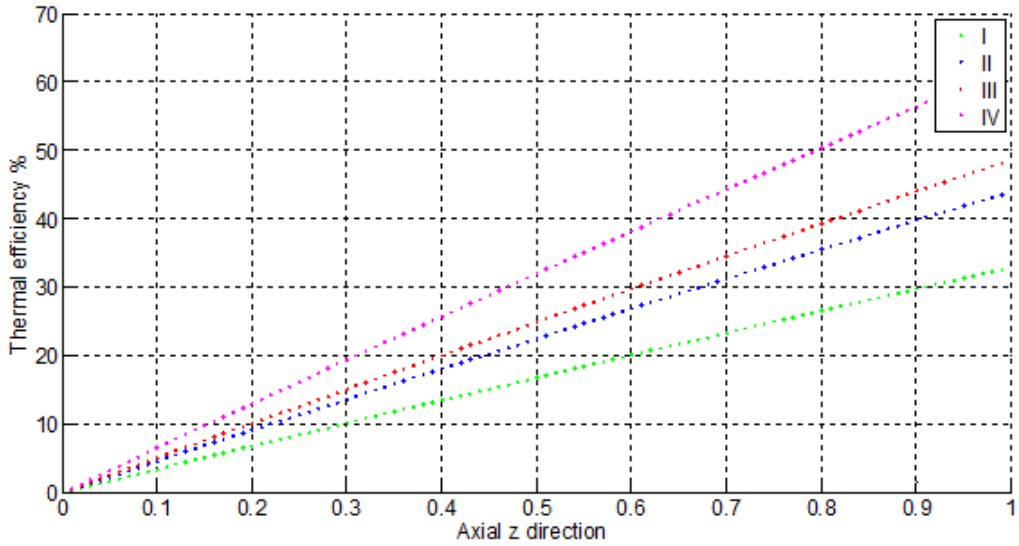

Figure 8. *Impact of mass flow rate on the thermal efficiency of the fluid in the flow direction. I-$\dot{m}$=9.5x10^{-3} kg/s II-$\dot{m}$=7.2x10^{-3} kg/s III-$\dot{m}$=6.9x10^{-3} kg/s IV-$\dot{m}$=5.8x10^{-3} kg/s.*

The curves in Figure 8 are straight lines that grow linearly in the direction of flow. For large values of the mass flow rate, the thermal efficiency of the fluid decreases.

On the one hand, figure 9 below shows the influence of the canopy width on the fluid temperature a function of time and figure 11 shows the influence of the canopy width on the thermal efficiency as a function of time. On the other hand, figure 10 shows the influence of the canopy width on the fluid temperature as a function of the axial direction and figure 12 shows the influence of the canopy width on the thermal efficiency as a function of the axial direction. Figure 9 and figure 11 have a parabolic shape while figure 12 and figure 14 have a linear shape. Figure 9 and figure 11 indicate that the fluid temperature and thermal efficiency increase as a function of time as the canopy width takes on larger and larger values. Figure 10 and figure 12 reveal that the fluid temperature and thermal efficiency increase as a function of axial direction for larger values of cover width.

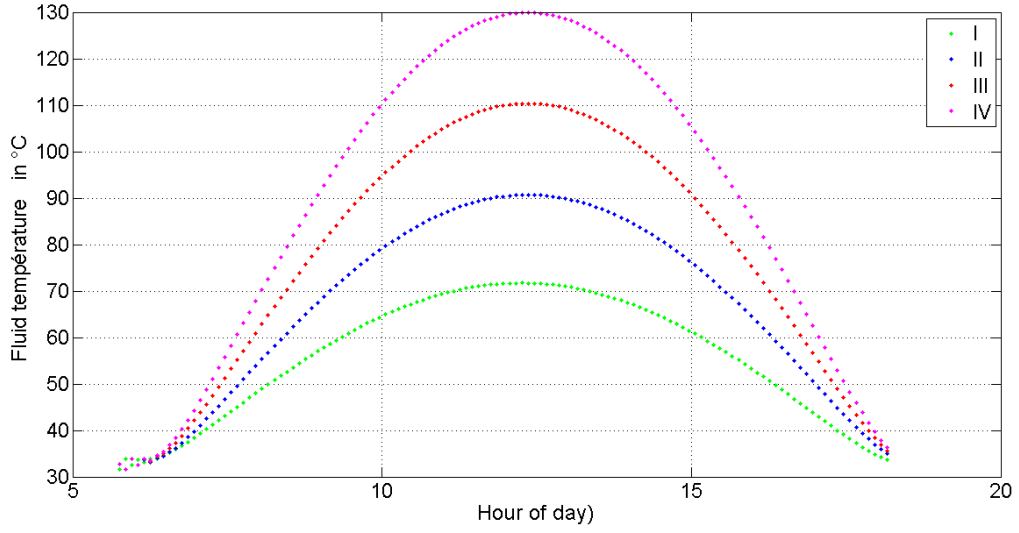

Figure 9. *Impact of canopy width on fluid temperature I-W=0.10m II-W=0.15m III-W=0.20m IV-W=0.25m.*

Figures 9, 10, 11 and 12 show that the greater the width of the canopy, the greater the fluid temperature and thermal efficiency. In order to have high temperature values, it is necessary to have a large canopy. The width of the canopy allows the maximum amount of solar radiation to pass over the absorber. If the width of the canopy is large, the number of solar rays that pass through the canopy is high.

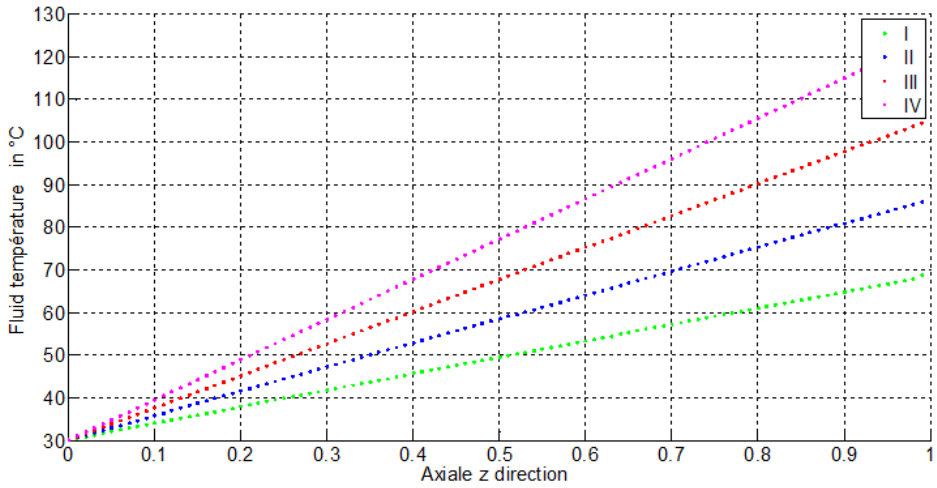

Figure 10. *Impact of canopy width on fluid temperature in the flow direction I-W=0.10m II-W=0.15m III-W=0.20m IV-W=0.25m.*

The nanofluid temperature of the curves in figure 10 varies with the axial z direction of the manifold. The highest curve corresponds to the one with the largest canopy width.

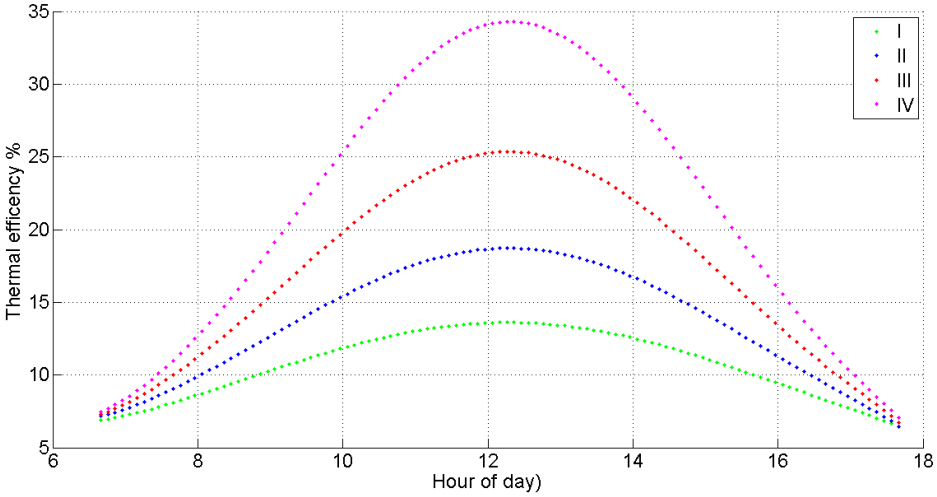

Figure 11. *Impact of canopy width on fluid thermal efficiency I-W=0.10m II-W=0.15m III-W=0.20m IV-W=0.25m.*

The thermal efficiency reaches its maximum at solar noon for all four curves in figure 11. The highest of the maximum values is for the one with the largest canopy width.

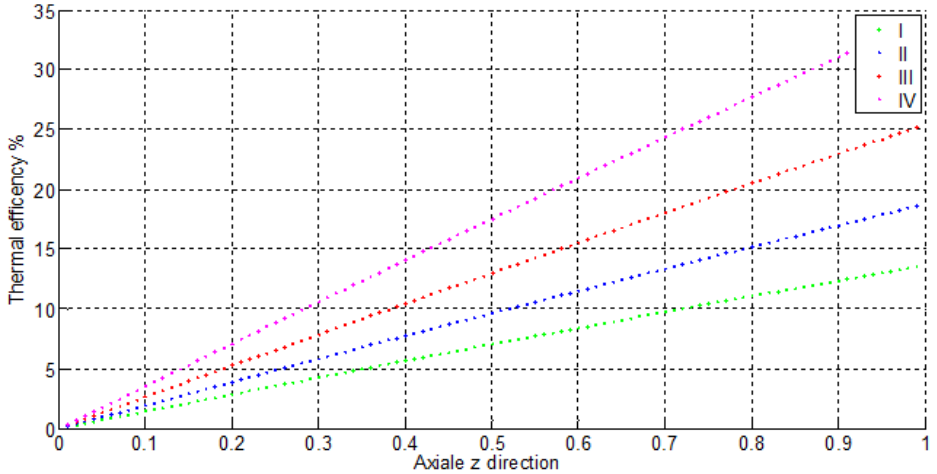

Figure 12. *Impact of canopy width on the thermal efficiency of the fluid in the flow direction I-W=0.10m II-W=0.15m III-W=0.20m IV-W=0.25m.*

The thermal efficiency of the collector is a function of the axial direction z of the flow. It reaches its maximum value at the end of the absorber tube of the solar collector. To obtain a high thermal efficiency value it is imperative to use a CPC with a large opening as shown in figure 12.

Figure 13 shows the evolution of the fluid temperature for four different opening angles. The greater the opening angle of the parabolic trough, the greater the temperature of the fluid. Indeed, the temperature of the fluid increases considerably because the device captures a maximum of energy knowing that the ambient temperature varies between 28 and 40°C, it is preferable to give the device an opening which allows it to capture a maximum of energy.

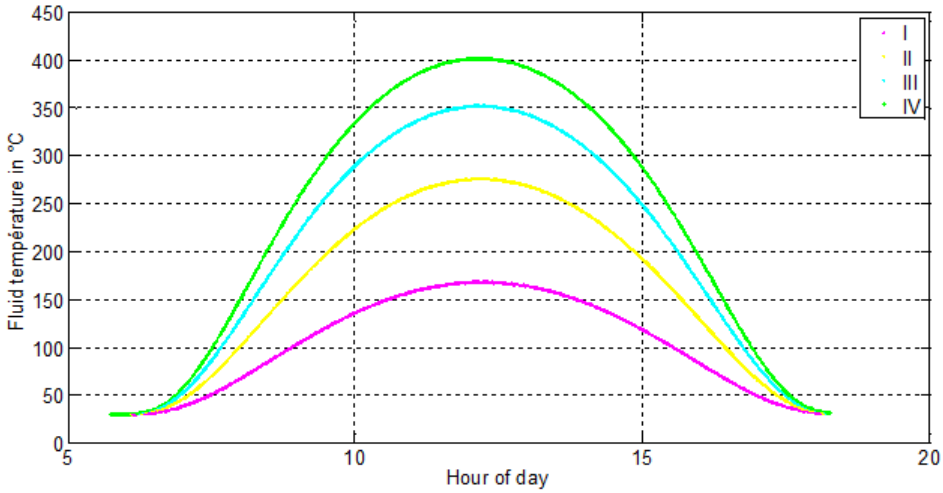

Figure 13. *Impact of the opening angle on the temperature of the fluid I-$\theta_c = 15°$; II-$\theta_c = 30°$; III-$\theta_c = 45°$; IV-$\theta_c = 60°$.*

The reflectance coefficient of the mirror affects the operation of the CPC. The higher its value, the higher the temperature becomes as shown in the figure 14. The choice of reflectors is very important to obtain very high temperatures of the fluid.

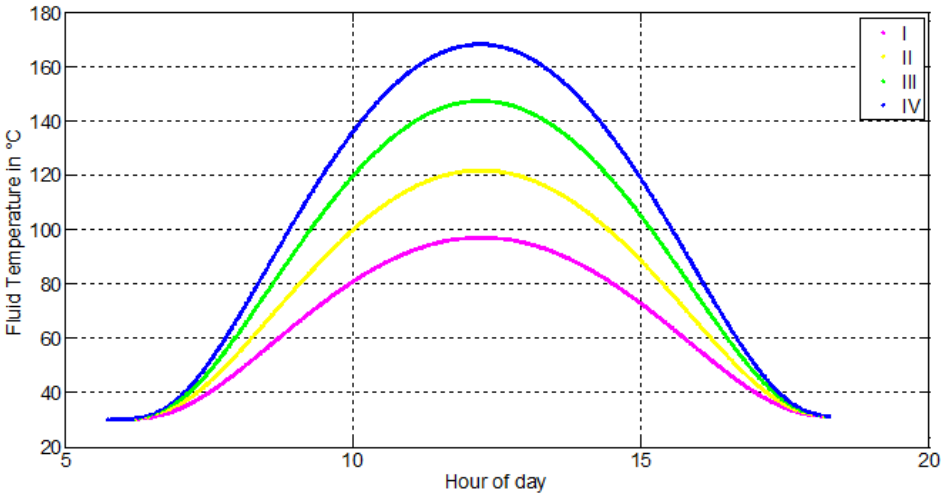

Figure 14. *Impact of the reflectance coefficient on the temperature of the fluid. I-$\rho_m = 0.5$; II-$\rho_m = 0.7$; III-$\rho_m = 0.85$; IV-$\rho_m = 0.95$.*

5. Conclusion

This paper presents a numerical simulation of the operating parameters of a CPC using a nanofluid as working fluid. It shows the behavior of the fluid outlet temperature and the thermal efficiency for different flow rates and for different values of the CPC canopy width. The numerical results indicate an interdependent relationship between the fluid mass flow rate, the fluid outlet temperature and the thermal efficiency of the CPC: the lower the mass flow rate, the higher the fluid outlet temperature and the thermal efficiency. In addition, there is an interdependent relationship between canopy width, fluid temperature and thermal efficiency: as the width increases, the fluid temperature and thermal efficiency increase. Also the opening angle and the reflectance coefficient have an influence on the CPC operation: the CPC outlet temperature increases with the opening angle and the reflectance coefficient of the CPC.

Nomenclature

Dimensioned numbers
Gr: Grashoff number
Nu: Nusselt number
Pr: Prandtl number
Re: Reynolds number
Greek letters
α: The absorption coefficient
ε: The emissivity
ζ: The reflectance coefficient
η: The efficiency of the concentrator
ϑ: The density, kg m^{-3}
ρ: The specific heat, J kg^{-1} K^{-1}
τ: The transmission coefficient
Latin letters
A: Surface area, m^2
C: The heat capacity, J kg^{-1} K^{-1}
$e_{f:}$ The distance between the bottom of the collector and the absorber plate, m
$e_{p\text{-}v}$: The space between the absorber plate and the glass, m
h: The transfer coefficient, Wm^{-2} K^{-1}
l: The width, m
L: The latent heat of vaporization, J kg^{-1} K^{-1}
M: The mass of the body, kg
$\dot{M}$: The mass flow rate, kg s^{-1}
n: The average reflection number
P: The pressure, bar
Q: The quantity of heat absorbed, J
Q_p: Power lost, W
T: The temperature, °C
t_c: Heating time, s
V: Wind speed, m/s
Indexes
c: Covered
c, c-v: Convective between the cover and the glass
c, p-f: Convective between the absorbing plate and the fluid
f: Fluid
fe: Finale
ie: Initiale
p: Absorbing plate
v: Glass
vap: Water vapour
u: Useful
r, c-v: Radiative between the canopy and the sky
r, c-sky: Radiative between the canopy and the sky
r, p-v: Radiative between the absorbing plate and the glass
Acronyms
CPC: Compound parabolic trough concentrator
DNI: Direct normal radiation, Wm^{-2}

Appendix

The thermo-physical properties of jatropha oil as a function of temperature expressed in °C have been expressed in the following table:

Table 1. *Thermophysical properties of jatropha oil.*

Characteristic	Formula	Unit
Density	$\rho_f = 933{,}47\ 7 - 0{,}7392T_f$	-
Heat capacity	$C_{pf} = 1{,}9608 + 0{,}441\ T_f + 12{,}947\ T_f^2$ - $10{,}423T_f^3$+$2{,}262T_f^4$	(J/Kg°C)
Thermal conductivity of jatropha oil	$\lambda_f = 0{,}1736$- $2{,}258T_f$+$2.80T_f^2$	$\left(\frac{W}{M}°C\right)$
Dynamic viscosity	$\mu_f = 32867\ T_f^{-1{,}8371}$	-

Table 2. *Characteristics of the concentrator.*

Component	Symbol	Value
Angle of acceptance (°)	θ_c	30
Canopy width (m)	W	0.25
Canopy length (m)	L_c	1
Canopy thickness (m)	ep_c	0.002
Length of glass (m)	L_c	1
Width of glass (m)	l_v	0.12
Thickness of glass (m)	ep_v	0.002
Absorber width (m)	l_p	0.10
Absorber length (m)	L_p	1
Absorber thickness (m)	ep_p	0.002
Insulator thickness (m)	ep_{is}	0.005

Table 3. *Thermophysical properties of reflectors.*

Physical properties	Symbol	Value
Reflectance of reflectors	ρ_m	0.92
The reflectance of the canopy	r_c	0.05
Reflectance of the flat absorber	r_p	0.15

Table 4. *Thermophysical properties of glasses.*

Physical properties	Symbol	Value
Density (kg.m^{-3})	ρ_v	1375
Mass heat capacity (J.kg^{-1}.K^{-1})	C_v	840
Thermal conductivity (W.m^{-1}.K^{-1})	λ_v	0,0263
Absorption coefficient of the glazing	α_v	0,05
Transmission coefficient of the glazing	τ_v	0,95

Table 5. *Thermophysical properties of absorber.*

Physical properties	Symbol	Value
Density (kg.m^{-3})	ρ_p	8900
Mass heat capacity (J.kg^{-1}.K^{-1})	C_p	398
Thermal conductivity (W.m^{-}1.K^{-1})	λ_p	384
Absorption coefficient of the absorber	α_p	0,98

Table 6. *Thermophysical properties of the insulation.*

Physical properties	Symbol	Value
Density (kg.m^{-3})	ρ_{is}	322,4
Mass heat (J.kg^{-1}.k^{-1})	C_{is}	272
Thermal conductivity (W.m^{-1}.k^{-1})	λ_{is}	0,108

References

[1] Gu X. T. R., M. G., Rosengarten G., Theoretical analysis of a novel portable, CPC-based solar thermal collector for methanol reforming. Applied Energy 119 465-475, 2014.

[2] Kerfouf Abd el Malek, F. M., Etude de transfert de chaleur de nanofluide dans une enceinte cylindrique 2020.

[3] Ahlam, G., Contribution à l'étude des transferts thermiques dans les nanofluides in Faculté des sciences de la Tehnologie, DEPARTEMENT DE GENIE MECANIQUE 2021: REPUBLIQUE ALGERIENNE DEMOCRATIQUE ET POPULAIRE.

[4] Çolak A. B., Y. O., Bayrak M., Tezekici B. S., Experimental Study For Predicting The Specific Heat Of Water Based Cu-Al_2O_3 Hybrid Nanofluid Using Artificial Neural Network And Proposing New Correlation. International Journal of Energy Research. 44: 7198-7215. 2020.

[5] Nguyen T. K., B. M. M., Ali J. A., Hamad S. M., Sheikholeslami M. et Shafee A., Macroscopic Modeling for Convection of Hybrid Nanofluid With Magnetic Effects. Physica A: Statistical Mechanics and its Applications, 534: 122136., 2019.

[6] Cimpean D. S., S. M. A., Pop I., Mixed Convection of Hybrid Nanofluid In a Porous Trapezoidal Chamber. International Communications in Heat and Mass Transfer 116: 104627., 2020.

[7] Adun H., W.-O. I., Okonkwo E. C., Bamisile O., Dagbasi M. et Abbasoglu S. (A Neural Network-Based Predictive Model For The Thermal Conductivity Of Hybrid Nanofluids. International Communications in Heat and Mass Transfer, 119: 104930., 2020.

[8] ROETZEL Y., X. W., Conception for heat transfer correlation of nanofluids. International Journal of Heat and Mass Transfer. 43 (19), 3701-3707, 2000.

[9] Pak B. C., Y. I. C., Hydrodynamic and heat transfer study of dispersed fluids with submicron metallic oxide particles. Experimental Heat Transfer. 11 151. 1998.

[10] Einstein., A., Eine neue bestimmung der molekul dimensionen. Annalen der Physik, 19. Leipzig, 1906: p. 289–306.

[11] H. C. Brinkman., The viscosity of concentrated suspensions and solution. Journal of Chemical Physics, 20., 1952: p. 571–81.

[12] G. K., B., The effect of Brownian motion on the bulk stress in a suspension of spherical particles. Journal of Fluid Mechanics. 83 (1). 1977: p. 97–117.

[13] Maiga S., P. S., Nguyen CT., Roy G., Galanis N., Heat transfer enhancement by using nanofluids in forced convection flows. International Journal of Heat and Fluid Flow. 26., 2005.: p. 530–46.

[14] Maxwell, J. C. A., Treatise on electricity and magnetism. Oxford, UK. Clarendon Press. 1881.

[15] Lu S., L. H., Effective conductivity of composites containing aligned spherical inclusions of finite conductivity. Journal of Applied Physics. 79: 6761–9., 1996.

[16] P. Keblinski, J. A. E., D. G. Cahill., Nanofluids for thermal transport. Materials today., 2005: p. 8-36.

[17] Timofeeva EV, G. A., McCloskey JM, Tolmachev YV., Thermal conductivity and particle agglomeration in alumina nanofluids: experiment and theory. Physical Review. 76: 061203, 2007.

[18] R. Tchinda, solved the governing equations of the energy to predicted the performance of air heater collector with the CPC having an absorber with flat plate. 2008.

[19] DUFFIE. J. A., B. W. A., Solar engineering of thermal processes, ed. é. 2nd. 1991, Wiley.

[20] Hsieh, C. K., Thermal analysis of CPC collectors. Elsevier Ltd, January 1981, Department of Mechanical Engineering, University of Florida.